Origin of luminescence from Ga_2O_3 nanostructures studied using x-ray absorption and luminescence spectroscopy

X. T. Zhou,[1] F. Heigl,[2] J. Y. P. Ko,[1] M. W. Murphy,[1] J. G. Zhou,[1] T. Regier,[3] R. I. R. Blyth,[3] and T. K. Sham[1,*]
[1]*Department of Chemistry, University of Western Ontario, London N6A 5B7, Canada*
[2]*Canadian Synchrotron Radiation Facility, Synchrotron Radiation Center, University of Wisconsin-Madison, Stoughton, Wisconsin 53589, USA*
[3]*Canadian Light Source, University of Saskatchewan, Saskatoon S7N 0X4, Canada*
(Received 13 June 2006; revised manuscript received 21 November 2006; published 2 March 2007)

The origin of the luminescence from Ga_2O_3 microcrystallites and nanostructures has been studied using time-resolved x-ray excited optical luminescence and x-ray absorption near-edge structure spectra in total electron yield and photoluminescence yield. The Ga_2O_3 nanostructures exhibit a crystalline β-Ga_2O_3 core and an amorphous oxide shell, an ultraviolet (UV) and a red emission with a shorter lifetime and a blue and a yellow emission with a longer lifetime when they are excited by x-ray. We suggest that the UV and red emissions from the Ga_2O_3 nanostructures are from the amorphous shell, while the blue and yellow emissions are from the crystalline β-Ga_2O_3 core; that the UV and red emissions are due to the presence of a subband of the amorphous Ga_2O_3, in the band gap. Our suggestion is in contrast to the previously proposed model, in which the UV emission from Ga_2O_3 is attributed to an intrinsic transition of crystalline β-Ga_2O_3. The implications of these observations are discussed.

DOI: 10.1103/PhysRevB.75.125303 PACS number(s): 78.67.−n, 61.46.−w, 61.10.Ht, 71.55.Gs

I. INTRODUCTION

Gallium oxide (Ga_2O_3) has five polymorphs, α, β, γ, δ, and ε. Among these polymorphs, β-Ga_2O_3 with a monoclinic structure is the only thermodynamically stable phase, while the others are metastable and the ε-Ga_2O_3 exhibits the lowest symmetry.[1] β-Ga_2O_3, a semiconductor with a wide band gap of 4.9 eV,[2] emits at a wide range of wavelengths from infrared to ultraviolet (UV).[3–6] This property makes it a candidate for gas sensing,[7] catalytic,[8] and optoelectronic devices[9] applications. Very recently, the study of the synthesis and optical properties of one-dimensional β-Ga_2O_3 nanostructures has attracted considerable interest due to the potential application of β-Ga_2O_3 nanowires in nanodevices. The luminescence from infrared to UV from β-Ga_2O_3 nanowires or nanoribbons has been widely reported.[4–6,10–26] The optical emission from one-dimensional β-Ga_2O_3 nanostructures depends on the deposition technique and experimental parameters. In many cases, both bulk β-Ga_2O_3 (Refs. 3 and 27–29) and β-Ga_2O_3 nanostructures[23–26] exhibit an UV (3.4 eV) and a broad blue emission. However, the origin of these emissions has not been clearly understood.

In the literature, the UV emission from β-Ga_2O_3 has been reported to be independent of sample history and impurity concentration and has thus been assigned to an intrinsic transition due to the recombination of an exciton with an electron below the bottom of conduction band (CB) and a trapped hole in the forbidden band gap; the blue and yellow emission bands have been attributed to the recombination of the electron-hole pair with an electron on a donor state formed by oxygen vacancy and a hole on an acceptor state formed by gallium vacancy.[3] Up to now, no direct experimental evidence has been provided to support the above model. Furthermore, the experimental results for the independence of the UV emission from β-Ga_2O_3 on sample history and impurity concentration cannot be explained satisfactorily by the above model.

In this work, we report the preparation and characterization of the structure, electronic properties and optical properties of β-Ga_2O_3 one-dimensional nanostructures using x-ray absorption near edge structure (XANES) and x-ray excited optical luminescence (XEOL) techniques. XANES is a technique that probes the unoccupied electronic densities of states above the Fermi level via electronic dipole transitions. XEOL is an x-ray photon-in, optical photon-out technique that monitors the optical response of light emitting materials excited by the absorption of x-ray photons. Upon x-ray excitation across an absorption edge of interest, XEOL can provide site and excitation channel specificity.[30–32]

Previous work on XEOL indicates that the photoluminescence yield (PLY) near an absorption threshold depends strongly on the site and the chemical environment of the absorbing atom; that is that the XANES in PLY provides valuable information about the origin of luminescence.[30] For instance, previous XEOL results from porous Si,[31] Si nanowires,[32] and ZnS nanoribbons[33] indicate that luminescence originated from different chemicals can be distinguished in the XEOL spectra. Time-gated XEOL tracks the decay of the emission bands and further provides new insight into the origin of the luminescence.[33–35] Here we present direct XANES and time-gated XEOL evidences to identify the luminescence sites responsible for UV and other emissions from Ga_2O_3 nanostructures.

II. EXPERIMENT

The Ga_2O_3 nanostructures were prepared by the thermal evaporation of a mixture of commercial Ga_2O_3 powders (99.99%, Alfa Aesar) and liquid Ga (1:1 in weight) in an alumina tube placed in a horizontal tube furnace system. A strip of *p*-type silicon wafer, having soaked in a hexane colloid containing thiol-capped gold nanoparticles with an average size of ~2 nm,[36] was placed downstream inside the

tube. The gold nanoparticles on the surface of the silicon wafer were used as catalyst. The nearly monodispersive Au nanoparticles provide a surface with uniformly coated Au nanoparticles. The tube was placed in a furnace and held at 950 °C for 2 hours. The carrier gas, Ar, was introduced at one end of the alumina tube at a flow rate of 100 sccm (standard cubic centimeters per minute), and the other end was open to air. After the reaction, a white film was found covering the Si substrate. Ga_2O_3 samples were analyzed by scanning electron microscopy (SEM, LEO 1530), transmission electron microscopy (TEM, JEOL 2010F), x-ray diffraction (XRD, Rigaku, Co K_α radiation, $\lambda=0.179$ nm) and UV-visible absorption (CARY 300 Bio UV visible spectrophotometer). X-ray absorption and XEOL experiments were conducted on the spherical grating monochromator (SGM) beamline (energy range, 250–1900 eV; $\Delta E/E$, $\sim 10^{-4}$) at the third generation, 2.9 GeV, Canadian Light Source (CLS) with an electron current of ~120 mA at injection. Timing experiments were conducted with one single electron bunch (~60 ps pulse width, 570 ns repetition rate, 15 mA current at injection). Time-resolved XEOL techniques have been reported elsewhere.[33–35] Briefly, a JY 100 monochromator (200–850 nm) equipped with a Hamamastu photomultiplier (PMT) was used to monitor the luminescence. The PMT signal (~2 ns response time) was used as the start and the bunch clock of the ring the stop; both signals were fed to a time to amplitude converter after appropriate amplification and discrimination, and the use of a suitable delay. The decay curve was stored in a multichannel analyzer. The time window used in time-gated measurements was set with the discriminator.

III. RESULTS AND DISCUSSION

From the SEM image of the Ga_2O_3 nanostructures shown in Fig. 1(a), we see a large amount of long wirelike and thin sheetlike nanostructures with thickness of tens of nanometer. TEM sample of the nanostructures was prepared by peeling off pieces of the nanostructure products from the Si substrate samples and placing them onto TEM copper grids with a carbon support film for observation. A typical TEM image of the nanostructures is shown in Fig. 1(b) at low magnification. Some very thin (tens of nm) nanowires or nanonribbons laid on the carbon supporting film are observed. The high resolution TEM image of a particular nanowire [Fig. 1(c)] clearly shows that the nanowire exhibits a core-shell structure, in which the core has a crystalline structure in β phase and the shell (~nm in thickness) is in amorphous phase (a phase).

XRD spectra [Fig. 2(a)] indicate that the nanostructures are predominantly crystalline β-Ga_2O_3, while the commercial Ga_2O_3 powder sample is a mixture of β-Ga_2O_3 and ε-Ga_2O_3.[1,37] The O K-edge and Ga $L_{3,2}$-edge XANES spectra of the Ga_2O_3 powder and nanostructure samples recorded in total electron yield (TEY) are displayed in Figs. 2(b) and 2(c), respectively. Clearly, the O K-edge XANES spectrum of the Ga_2O_3 nanostructure sample is quite different from that of the Ga_2O_3 powder [Fig. 2(b)]. For the nanostructure sample, its TEY-XANES spectrum exhibits two main peaks, A_1 and A_2, a pattern similar to that of the β-Ga_2O_3 powders

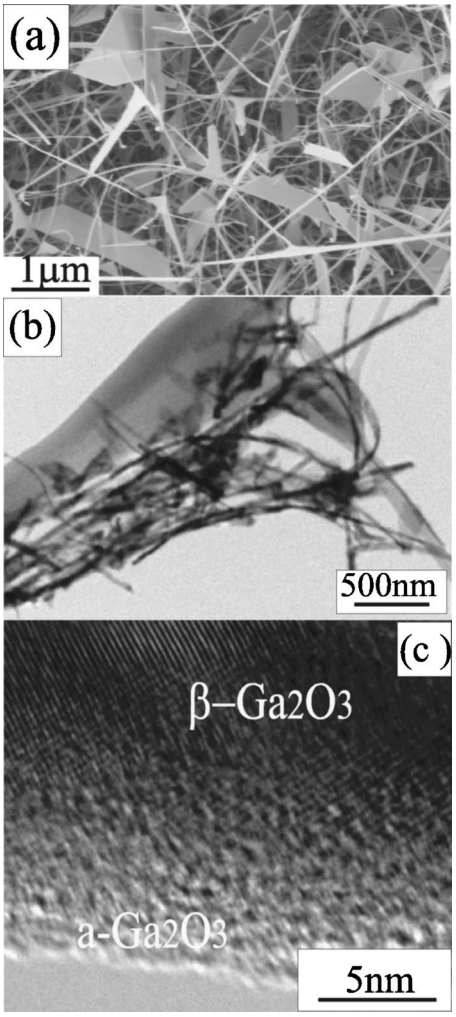

FIG. 1. (a) SEM and (b) TEM images of a Ga_2O_3 nanostructure sample, and (c) HRTEM image of a particular Ga_2O_3 nanowire.

reported in the literature.[38] For the commercial Ga_2O_3 powder sample, besides the main peak A_1 as seen in the nanostructure one, its TEY-XANES spectrum also exhibits a distinct pre-edge feature A_3, which is absent for the Ga_2O_3 nanostructure sample in the β phase. The crystal structure of β-Ga_2O_3 is depicted in Fig. 2(d). It is worth noting that in the β-phase, oxygen atoms occupy both octahedral and tetrahedral sites forming octahedral and tetrahedral polygons by sharing the corners. The crystal structure of the ε phase is not known. A recent extended x-ray absorption fine structure (EXAFS) analysis shows that the ratio of the coordination number, Ga (tetrahedral)/Ga (octahedral) in the β phase decreases as the particles size decreases and decreases further in the ε phase. The radial distribution from the Fourier transform of the EXAFS data shows some similarity between the two with significant reduction in the amplitude of the second shell indicating that there is considerable long-range order degradation in the ε phase.[38] Here, we believe that the difference of the O K-edge TEY-XANES spectra shown in Fig. 2(b) between the above two samples and the pre-edge feature (A_3) for the powder sample arise from the existence of an energy state in the band gap and we attribute the origin of the feature A_3 to the ε-Ga_2O_3 in the powder sample. On the

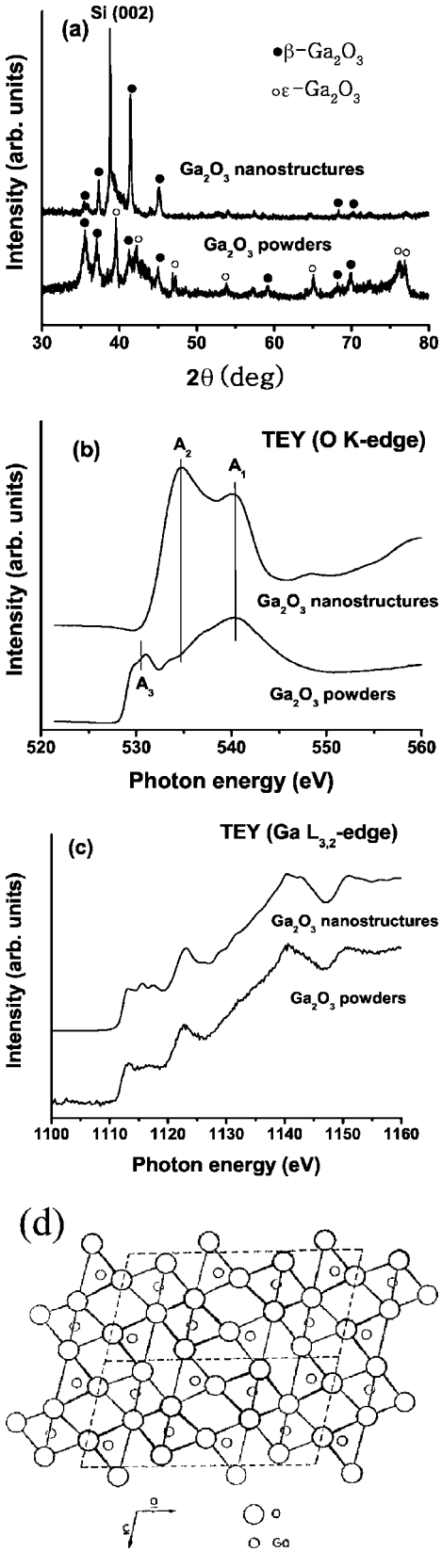

FIG. 2. (a) XRD patterns, (b) O *K*-edge, and (c) Ga $L_{3,2}$-edge TEY-XANES spectra of the Ga_2O_3 nanorstructure and commercial powder samples, and (d) the schematic of the crystal structure of β-Ga_2O_3. The solid and open circles in (a) represent β-Ga_2O_3 and ε-Ga_2O_3, respectively.

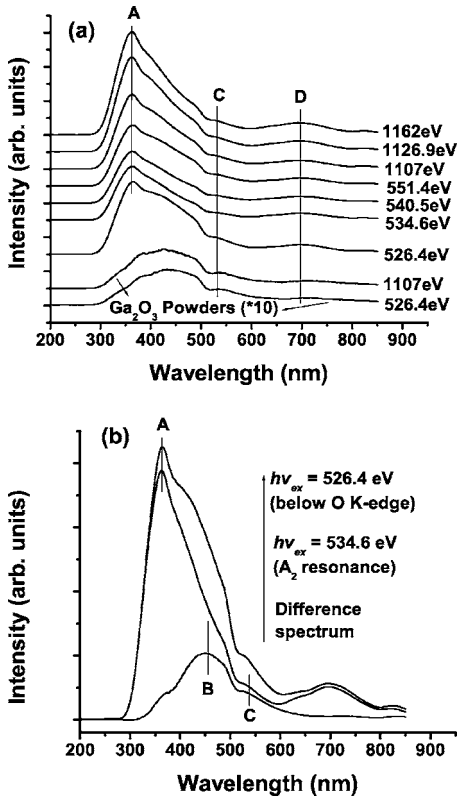

FIG. 3. (a) Room temperature XEOL spectra of the nanostructure sample (normalized to photon flux) excited at several photon energies across the O *K*-edge and Ga $L_{3,2}$-edge and (b) XEOL spectra of the nanostructure sample with excitation below and at resonance of the O *K*-edge. The difference curve is also shown.

other hand, the Ga $L_{3,2}$-edge XANES spectra of these two samples are very similar to that of β-Ga_2O_3 reported in literature,[39] indicating that the local environments of Ga atom of the Ga_2O_3 in the above two phases are similar on average [Fig. 2(c)], although there are subtle differences. (For instance, the powder features are more blurry.) All the experimental results shown in Fig. 2 demonstrate that the nanostructures are predominantly crystalline β-Ga_2O_3, while the starting material, the powder sample, is a mixture of β-Ga_2O_3 and ε-Ga_2O_3. For the nanostructure sample, no noticeable amorphous Ga_2O_3 (a-Ga_2O_3) was detected by the XRD and XANES spectra (Fig. 2), although a-Ga_2O_3 was indeed observed by high resolution TEM image [Fig. 1(c)]. The reason should be that the a-Ga_2O_3 in the nanostructure sample is too dilute to be detected by XRD and TEY-XANES techniques. Additionally, the XRD is not an amorphous materials-sensitive technique.

The room temperature XEOL spectra from the Ga_2O_3 nanorstructure and power samples excited with photon energies near the O *K*-edge (526.4–551.4 eV) and the Ga $L_{3,2}$-edge (1107–1162 eV) are shown in Fig. 3(a). The nanostructure sample exhibits a strong UV emission, band *A*, at 365 nm (3.41 eV) and two weak emissions, band *C* (yellow) at 528 nm (2.35 eV), and band *D* (red) at ~700 nm (1.78 eV). A shoulder in the blue range can be clearly observed from the XEOL spectrum when the nanostructure sample was excited by the x-ray with the energy of 526.4 eV

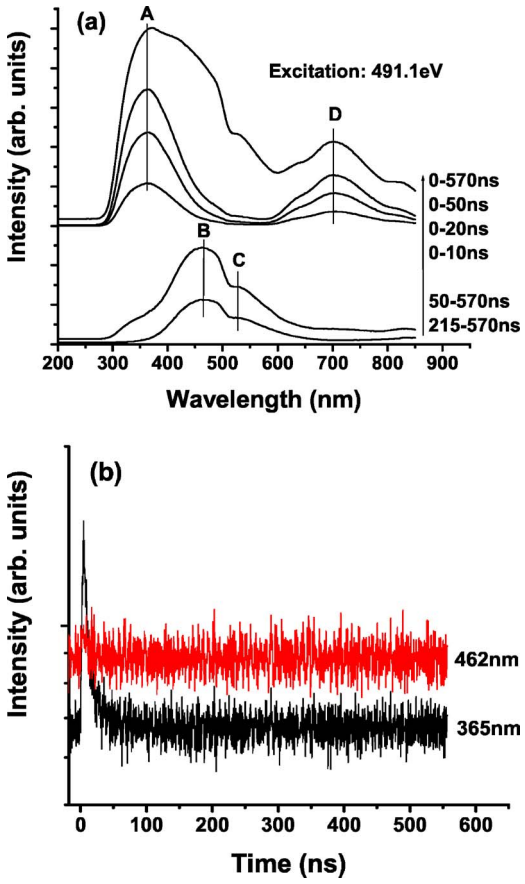

FIG. 4. (Color online) (a) Time-resolved XEOL spectra of the Ga_2O_3 nanostructure sample excited at 491.9 eV photon energy and collected with selected time windows and (b) decay behaviors of the emission bands *A* and *B* shown in (a); note that the time is reversed relative to the experimental setup and the noise appears enhanced in the log plot.

(below O *K*-edge). The dramatic difference in emission features for excitations just below and at the O *K*-edge resonance is shown in Fig. 3(b) where we can clearly see the marked decrease in intensity in the 400–500 nm region. The difference spectrum clearly shows features in this blue region, which was blurred when excited at the resonance (A_2). We denote the peak revealed at ~450 nm in the difference spectrum *B*. Peak *C* as seen in Fig. 3(a) is now enhanced. These emission bands have been observed for both Ga_2O_3 nanostructures and bulk[3,23–29] and will have significant bearings on the interpretation of the time-resolved results discussed below.

Figure 4(a) shows the time-gated XEOL spectra from the Ga_2O_3 nanostructure sample excited at 491.1 eV (below the O *K*-edge) with selected time window settings where 0–10, 0–20, and 0–50 ns represents fast windows, 50–570, 215–570 ns represents slow windows, and the 0–570 ns setting a fully open window (ungated). We selected the excitation energy below the O *K*-edge because luminescence in the blue region is intense at these energies. The most interesting feature displayed in Fig. 4(a) is that a blue emission band *B* centered at 462 nm (2.69 eV), together with band *C*, emerge in the slow window-gated XEOL (50–570 ns, 215–570 ns) and disappears in the fast windows (0–10 ns, 0–20 ns, and 0–50 ns). It should be noted that the slow window XEOL featuring emission bands *B* and *C* are nearly the same as the difference curve shown in Fig. 3(b). The slow decay indicates long lifetime associated with trapped excitons or defect states. Returning to Fig. 3(b), we now attribute the excitation-energy sensitive XEOL to excitation channel specificity. Below the O *K*-edge, only the valence and inner valence states are excited. At the O *K*-edge the 1*s* excitation turns on, this will have an effect on the optical photon yield. Judging from Fig. 3(b) and Fig. 4(a), we conclude that the yield is much greater with excitation energy below the O *K*-edge than above the edge. This observation indicates that the PLY at the O *K*-edge XANES will likely be inverted. As we will show below, this is indeed the case.

Figure 4(a) also shows that emission bands *A* and *D* are diminishing in the slow windows but become more intense in the fast windows. The decay curves of the two strong emission bands in Fig. 4(b) confirm that the UV emission exhibits a very fast decay (<ns), which is faster than the time resolution of the PMT (~2 ns), while the blue emission exhibits a much slower decay behavior; the lifetime is too long ($>\mu$s) to be estimated precisely due to the limitation of the ungated time window (570 ns). The very short lifetime (<ns) of the UV and red emissions indicates the involvement of nonradiative transition to the process. All these experimental results indicate that the origin of bands *A* and *D* is distinctly different from that of bands *B* and *C*. From Figs. 3 and 4, we see that both the Ga_2O_3 nanostructure and the powder samples exhibit blue, yellow, and red emissions. Note that the Ga_2O_3 nanostructure sample exhibits a much stronger luminescence (~ a factor of 10), especially for the UV emission (3.4 eV), compared to the powder.

The O *K*-edge and Ga $L_{3,2}$-edge XANES spectra recorded in TEY and PLY (optical channel-selected at 383 nm, 426 nm, and zero order) of the Ga_2O_3 powder sample are displayed in Figs. 5(a) and 5(b), respectively. It should be noted that the O *K*-edge PLY-XANES spectra [inset of Fig. 5(a)] exhibit an inverted edge jump. Inversion in a PLY spectrum is not uncommon in soft x-ray optical XANES spectra when the sample is thick or the excited state turned on by the absorption at the edge has a less efficient optical decay.[30] In order to compare the XANES spectra in different yields, we plot the inverted PLY spectra for the two channels (383 nm and 426 nm) and zero order in Fig. 5(a). We see that the inverted PLY spectra have similar spectral features to the TEY one, for instance, the distinct pre-edge feature A_3 and two stronger features A_1 and A_2 are all observed. This reveals that the luminescence from the Ga_2O_3 powders comes from Ga_2O_3 in both β and ε phases. The well-defined features A_2 and A_3 in the PLY spectra indicate the contribution of the β and ε phases, respectively, to the luminescence. The similarity of the Ga $L_{3,2}$-edge PLY- (0 order) and TEY-XANES spectra of the powder sample indicates that the observed luminescence is proportional to the absorption at the Ga $L_{3,2}$-edge of Ga_2O_3 [Fig. 5(b)].

The O *K*-edge and Ga $L_{3,2}$-edge XANES spectra recorded in TEY and PLY (optical channel-selected at 363 nm, 485 nm, 524 nm, 699 nm and zero order) of the Ga_2O_3 nano-

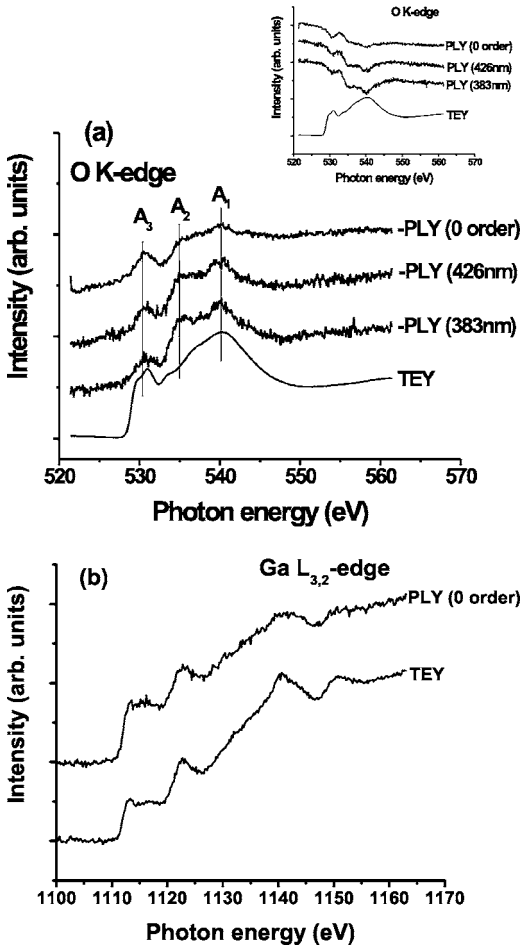

FIG. 5. (a) The O *K*-edge and (b) Ga $L_{3,2}$-edge XANES spectra of the Ga_2O_3 powder sample obtained in TEY and PLY. Note that the PLY-XANES spectra are inverted at the edge [inset of (a)]. The inverted PLY spectra are plotted with the TEY one for comparison. The intensities in TEY and PLY spectra are the quantity of Auger electron and secondary electron and the intensity of optical luminescence emitted from sample excited by x-ray, respectively.

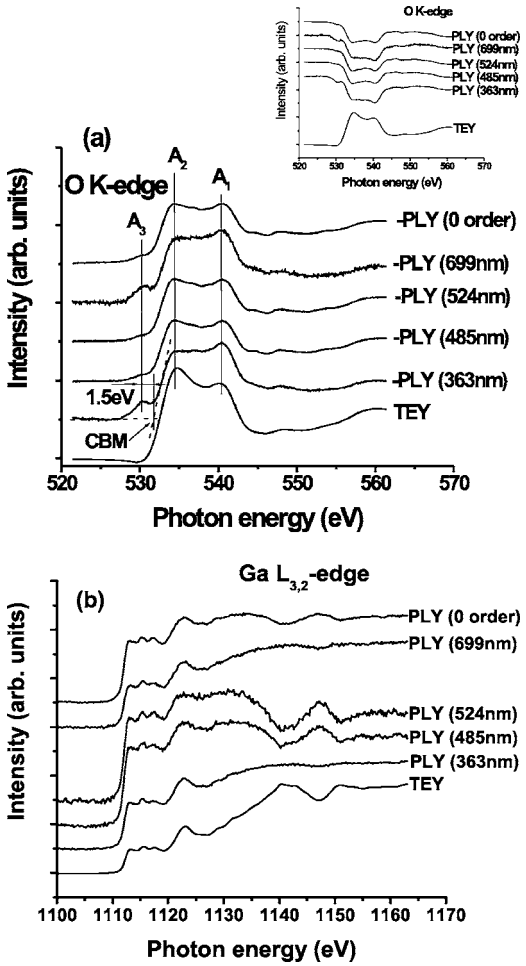

FIG. 6. (a) The O *K*-edge and (b) Ga $L_{3,2}$-edge XANES spectra of the Ga_2O_3 nanostructure sample obtained in TEY and in PLY. Note that the PLY-XANES spectra are inverted at the O *K*-edge [inset of (a)]. The inverted PLY spectra are plotted with the TEY one for comparison.

structure sample are displayed in Figs. 6(a) and 6(b), respectively. The O *K*-edge XANES spectra in PLY [inset of Fig. 6(a)] also exhibit an inverted edge jump. The inverted PLY spectra of the blue and yellow emissions, 485 nm and 524 nm, respectively, have similar spectral features compared to that of the TEY one of β-Ga_2O_3 (A_2 and A_1 with no noticeable pre-edge feature A_3), while those of the UV and red emissions, 363 nm and 699 nm, respectively, are more similar to the PLY ones of the luminescence from the Ga_2O_3 powder sample shown in Fig. 5(a). From the O *K*-edge PLY-XANES spectra in Fig. 6(a), the most noticeable feature is the appearance of A_3. We can also determine that the position of the feature A_3, relative to the conduction band minimum (CBM), is centered at ~1.5 eV below the CBM. CBM is determined by extrapolating the linear part of the absorption edge just above the threshold to its intersection with the baseline extrapolation of the pre-edge.[40,41] The appearance of A_3 of the PLY spectra [Fig. 6(a)] reveals that a subband in the band gap is involved in the optical transition responsible for the emissions *A* and *D*.[41] Incidentally, the powder containing ε-Ga_2O_3 also exhibits the pre-edge feature A_3 at the same position [Fig. 5(a) and Fig. 6(a)]. This observation implies that the luminescence in blue and yellow are from the crystalline β-phase and that the UV and red emission are from *a* phase (see below). The similarity of the Ga $L_{3,2}$-edge PLY- and TEY-XANES spectra for the nanostructures sample also confirms that the observed luminescence comes from Ga_2O_3 [Fig. 6(b)]. Close observation reveals that all the Ga $L_{3,2}$-edge PLY spectra exhibit a normal edge jump with the exception of the Ga L_2-edge PLY spectra of blue and yellow emissions, 485 nm and 524 nm, respectively, which exhibit an inverted edge jump, while the Ga L_2-edge PLY ones of the UV and red emissions (363 nm and 699 nm, respectively) a much smaller normal one, relative to their corresponding L_3-edge PLY ones. This may be due to the switch on of the Coster-Kronig transition at the L_2-edge, leading to a different deexcitation pathway, which affects the energy transfer to the optical channel. The difference of the Ga L_2-edge jump of the nanostructure sample between the emission bands [Fig. 6(b)] reveals the different luminescence site position for the emission bands from the nanostructures. The normal edge

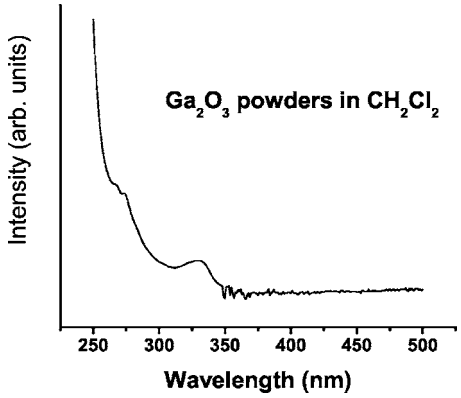

FIG. 7. UV-visible absorption spectrum of the Ga_2O_3 powders suspended in CH_2Cl_2 solvent.

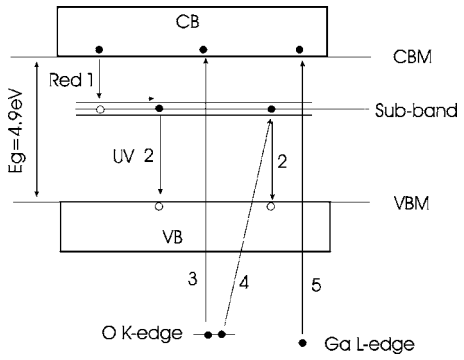

FIG. 8. Schematic diagram for the excitation and relaxation processes of the UV and red emissions from a-Ga_2O_3. The solid and open circles in Fig. 7(b) represent electrons and holes, respectively. The arrows in Fig. 7(b) indicate excitation or emission processes. Relevant processes are labeled 1–5 (see text).

jump for the UV and red emissions reveals that their luminescence sites are mainly located at near-surface region (negligible thickness effect), while the inverted one for the blue and yellow bands indicates that their luminescence sites are mainly from the bulk of the nanostructures (more severe thickness effect).[30,42,43]

We now assign the luminescence bands A, B, C, and D from the Ga_2O_3 nanostructures. Here, we suggest that the blue and yellow emissions, B and C, come from the crystalline β-Ga_2O_3 core [Fig. 1(c)] of the nanostructures. The similarity of the O K-edge XANES spectra in PLY of these two emission bands and in TEY of the Ga_2O_3 nanostructure sample [Fig. 6(a)] confirms this point. In addition, their inverted jump of the Ga L_2-edge PLY [Fig. 6(b)] also demonstrates that these two emissions are more bulklike, relative to the emissions A and D. In other words, the luminescence sites responsible for these two emissions should be at the core of the nanostructures. This is also evident from the high resolution TEM image [Fig. 1(c)] which shows the crystalline β-Ga_2O_3 core is shelled by an amorphous outer layer. We further assign these two emissions to a recombination of the electron-hole pair with a deeply trapped electron on a donor state forming the oxygen vacancy and a deeply trapped hole on an acceptor state forming the gallium vacancy.[3] The luminescence from the deeply defect trapped electron-hole pairs must come from β-Ga_2O_3 and decays very slowly because of the long lifetime of the trapped electron-hole pairs, which is also confirmed by our experimental results (Fig. 4).

For the UV and red emissions (A and D, respectively), our results indicate that they are probably from an impurity phase rather than the dominantly crystalline β phase. The appearance of the pre-edge feature at the O K-edge of Ga_2O_3 powder containing ε-Ga_2O_3 [Fig. 2(a)] indicates the presence of an unoccupied state in the forbidden band gap. This intrinsic unoccupied state probably arises from the structural effect, e.g., poor long-range order. Existing experimental results suggest that the long-range order of ε-Ga_2O_3 is degradated, compared to the β phase, although its structure has not been fully characterized. This subband of ε-Ga_2O_3 is also observed by an UV-visible absorption spectrum of the Ga_2O_3 powders suspended in a CH_2Cl_2 solvent shown in Fig. 7, where a feature peaked at 331 nm (3.76 eV) is observed in the UV-visible absorption spectrum, which suggests the existence of a subband located at ~3.76 eV (or a little bit below this position) above the valance band maximum (VBM) in the forbidden band of ε-Ga_2O_3, as the previous UV-visible absorption results in literature show that β-Ga_2O_3 does not exhibit this additional feature.[2] The position of this subband related to the poor long-range order of the ε-Ga_2O_3 estimated from the XANES spectra of the powder sample [the same position as the impurity phase in the nanostructure sample, Fig. 5(a)] is in good accord with the UV-visible absorption spectrum (Fig. 7), assuming that all phases have similar band gaps (~4.9 eV). Here, we suggest that the UV and red emissions from the nanostructure sample come from the amorphous shell of the nanostructures [Fig. 1(c)]. The lack of long-range order of the a phase and the inverted edge jump of the Ga L_2-edge PLY spectrum [Fig. 6(b)] are consistent with this notion. Actually, an UV emission, together with a blue one, from a-Ga_2O_3 nanowires has been reported.[23] Furthermore, we believe that the impurity a phase is much more luminescent than the dominant β phase. When the excitation x-ray is scanned to A_3, only the a phase gets a fluorescence deexcitation channel and we observe that the yield of the luminescence from the more luminescent a phase changes. However, the impurity a phase is so dilute that it cannot be detected from TEY spectrum, although it indeed absorbs x-ray and gets a fluorescence deexcitation channel. On the contrary, the disappearance of the A_3 in the TEY spectrum does indicate that the UV and red emissions come from the impurity phase, not from the dominant one.

Based on the above experimental results and the position of the subband shown in Fig. 6(a), a scheme of the energy band structure of a-Ga_2O_3 is proposed (Fig. 8). After the amorphous shell of nanostructures is excited by x-ray (e.g., processes 3 and 5), relaxation of the energetic electrons and the holes ($<$ ps) and thermalization (~1–10 ps) take place, which populates electrons and holes in the CB and VB, respectively.[44] The electrons in the CB can transfer to the subband radiatively (process 1), leading to the emission in red, or decay nonradiatively. Thus, we can assign the red emission (band D) to process 1. Other electrons in the subband may come from the core level (process 4) or the VB

due to the excitation of x-ray. The electron in the subband is not stable and will decay radiatively (process 2) or nonradiatively. We assign the UV emission (band *A*) to a radiative channel, process 2. In other words, the radiative process 1 responsible for red emission and process 2 for UV can be regarded as the two steps of so-called cascade emission. As some of the electrons in the subband come from the core level (process 4) or the VB, the intensity of UV emission is expected to be stronger than the red one, which is confirmed experimentally. The sum of the energies at the peak position of UV and red emissions (3.42 eV+1.78 eV=5.20 eV) is very close to the band gap of Ga_2O_3 (4.9 eV). In addition, the electron in the subband belongs to the whole a-Ga_2O_3 shell and thus has a much shorter lifetime, relative to the defect-trapped electron in the β-Ga_2O_3 core. The match between the above energy sum and the band gap of Ga_2O_3 and the quick decay behavior of UV and red emissions support the above assignments. Another possibility about the origin of the red emission from the nanostructures is that some of the red luminescence, especially for the red luminescence with longer wavelength, is probably the higher order of the UV emission, as the red emission exhibits a wide peak and the positions of the red luminescence with longer wavelength are double of those of the UV luminescence [Fig. 4(a)]. Recently, Song *et al.* reported emission in the red at ~700 nm with lifetime in the order of 10^2 μs from nitrogen doped Ga_2O_3 nanowires, and assigned this emission to the recombination of the deeply trapped exciton.[6] Obviously, emission in the red from our Ga_2O_3 nanostructure sample has a much shorter lifetime (<1 ns) and thus has a different origin.

IV. CONCLUSIONS

The Ga_2O_3 nanostructures exhibit a crystalline β-Ga_2O_3 core and an amorphous oxide shell, an UV and a red emission with a shorter lifetime, and a blue and a yellow emission with a longer lifetime when they are excited by x-ray. We suggest that the luminescence site responsible for the UV and red emissions from Ga_2O_3 nanostructures is their amorphous outer shell, while that for the blue and yellow emissions is their crystalline β-Ga_2O_3 core; that the UV and red emissions are due to the presence of the intrinsic subband in the band gap of a-Ga_2O_3.

ACKNOWLEDGMENTS

Research at the University of Western Ontario was supported by NSERC and CRC for one of the authors (T.K.S.). CLS is supported by NSERC, NRC, CIHR, and the University of Saskatchewan. The TEM images were obtained at the Brockhouse Institute for Materials Research, McMaster University; the assistance of Carmen Andrei is acknowledged.

*Author to whom correspondence should be addressed. Electronic address: sham@uwo.ca

[1] R. Roy, V. G. Hill, and E. F. Osborn, J. Am. Chem. Soc. **74**, 719 (1952).
[2] H. H. Tippins, Phys. Rev. **140**, A316 (1965).
[3] L. Binet and D. Gourier, J. Phys. Chem. Solids **59**, 1241 (1998).
[4] C. H. Liang, G. W. Meng, G. Z. Wang, Y. W. Wang, and L. D. Zhang, Appl. Phys. Lett. **78**, 3202 (2001).
[5] E. Nogales, B. Mendez, and J. Piqueras, Appl. Phys. Lett. **86**, 113112 (2005).
[6] Y. P. Song, H. Z. Zhang, C. Lin, Y. W. Zhu, G. H. Li, F. H. Yang, and D. P. Yu, Phys. Rev. B **69**, 075304 (2004).
[7] M. Fleisher and H. Meixner, Sens. Actuators B **4**, 437 (1991).
[8] A. L. Petre, A. Auroux, P. Gelin, M. Caldararu, and N. I. Ionescu, Thermochim. Acta **379**, 177 (2001).
[9] T. Miyata, T. Nakatani, and T. Minami, J. Lumin. **87-89**, 1183 (2000).
[10] P. C. Chang, Z. Y. Fan, W. Y. Tseng, A. Rajagopal, and J. G. Lu, Appl. Phys. Lett. **87**, 222102 (2005).
[11] X. Xiang, C. B. Cao, and H. S. Zhu, J. Cryst. Growth **279**, 122 (2005).
[12] N. H. Kim and H. W. Kim, Appl. Surf. Sci. **242**, 29 (2005).
[13] S. Sharma and M. K. Sunkara, J. Am. Chem. Soc. **124**, 12288 (2002).
[14] G. Gundiah, A. Govindaraj, and C. N. R. Rao, Chem. Phys. Lett. **351**, 189 (2002).
[15] H. W. Kim and N. H. Kim, Appl. Phys. A: Mater. Sci. Process. **A80**, 537 (2005).
[16] L. Fu, Y. Q. Liu, P. A. Hu, K. Xiao, G. Yu, and D. B. Zhu, Chem. Mater. **15**, 4287 (2003).
[17] J. Hu, Q. Li, X. M. Meng, C. S. Lee, and S. T. Lee, J. Phys. Chem. B **106**, 9536 (2002).
[18] K. W. Chang and J. J. Wu, Appl. Phys. A: Mater. Sci. Process. **76**, 629 (2003).
[19] J. Zhang and F. H. Jiang, Chem. Phys. **289**, 243 (2003).
[20] J. Zhang, F. H. Jiang, and L. D. Zhang, Phys. Lett. A **322**, 363 (2004).
[21] X. C. Wu, W. H. Song, W. D. Hung, M. H. Pu, B. Zhao, Y. P. Sun, and J. J. Du, Chem. Phys. Lett. **328**, 5 (2000).
[22] H. J. Chun, Y. S. Choi, S. Y. Bae, H. W. Seo, S. J. Hong, J. H. Park, and H. Yang, J. Phys. Chem. B **107**, 9042 (2003).
[23] N. H. Kim, H. W. Kim, C. Seoul, and C. Lee, Mater. Sci. Eng., B **111**, 131 (2004).
[24] P. Guha, S. Chakrabarti, and S. Chaudhuri, Physica E (Amsterdam) **23**, 81 (2005).
[25] H. W. Kim, N. H. Kim, and C. M. Lee, J. Mater. Sci.: Mater. Electron. **16**, 103 (2005).
[26] K. W. Chang and J. J. Wu, Adv. Mater. (Weinheim, Ger.) **16**, 545 (2004).
[27] S. Y. Cho, J. W. Lee, I. Y. Park, and S. T. Kim, Mater. Lett. **57**, 1004 (2002).
[28] H. W. Kim and N. H. Kim, Appl. Surf. Sci. **230**, 301 (2004).
[29] E. G. Villora, K. Hatanaka, H. Odaka, T. Sugawara, T. Miura, H. Fukumura, and T. Fkada, Solid State Commun. **127**, 385 (2003).
[30] A. Rogalev and J. Goulon, in *Chemical Applications of Synchotron Radiation*, edited by Tsun-Kong Sham (World Scientific, Singapore, 2002), p. 707.
[31] T. K. Sham, D. T. Jiang, I. Coulthard, J. W. Lorimer, X. H. Feng,

K. H. Tan, S. P. Frigo, R. A. Rosenberg, D. C. Houghton, and B. Bryskiewicz, Nature (London) **363**, 332 (1993).

[32] T. K. Sham, S. J. Naftel, P. S. G. Kim, R. Sammynaiken, Y. H. Tang, I. Coulthard, A. Moewes, J. W. Freeland, Y. F. Hu, and S. T. Lee, Phys. Rev. B **70**, 045313 (2004).

[33] R. A. Rosenberg, G. K. Shenoy, F. Heigl, S. T. Lee, P. S. G. Kim, X. T. Zhou, and T. K. Sham, Appl. Phys. Lett. **86**, 263115 (2005).

[34] F. Heigl, S. Lam, T. Regier, I. Coulthard, and T. K. Sham, J. Am. Chem. Soc. **128**, 3906 (2006).

[35] F. Heigl, A. Juergensen, X. T. Zhou, S. Lam, M. Murphy, J. Y. P. Ko, T. K. Sham, R. A. Rosenberg, R. Gordon, D. Brewe, T. Regier, and L. Armelao, SRI2006, Korea.

[36] P. Zhang and T. K. Sham, Appl. Phys. Lett. **81**, 736 (2002).

[37] K. Nishi, K. I. Shimizu, M. Takamatsu, H. Yoshida, A. Satsuma, T. Tanaka, S. Yoshida, and T. Hattori, J. Phys. Chem. B **102**, 10190 (1998).

[38] F. Tourtin, P. Armand, A. Ibanez, G. Tourillon, and E. Philippot, Thin Solid Films **332**, 85 (1998).

[39] K. Shimizu, M. Takamatsu, K. Nishi, H. Yoshida, A. Satsuma, and T. Hattori, Chem. Commun. (Cambridge) **1996**, 1827 (1996).

[40] T. van Buuren, L. N. Dinh, L. L. Chase, W. J. Siekhaus, and L. J. Terminello, Phys. Rev. Lett. **80**, 3803 (1998).

[41] X. T. Zhou, F. Heigl, M. W. Murphy, T. K. Sham, T. Regier, I. Coulthard, and R. I. R. Blyth, Appl. Phys. Lett. **89**, 213109 (2006).

[42] S. Emura, T. Moriga, J. Takizawa, M. Nomura, K. R. Bauchspiess, T. Murata, K. Harada, and H. Maeda, Phys. Rev. B **47**, 6918 (1993).

[43] D. T. Jiang, I. Coulthard, T. K. Sham, J. W. Lorimer, X. H. Feng, and R. A. Rosenberg, J. Appl. Phys. **74**, 6335 (1993).

[44] P. A. Rodnyi, *Physical Processes in Inorganic Scintillators* (CRC Press, New York, 1997).